

An Efficient Spectral-Projection Method for the Navier–Stokes Equations in Cylindrical Geometries

II. Three-Dimensional Cases

J. M. Lopez,* F. Marques,† and Jie Shen‡

**Department of Mathematics, Arizona State University; †Departament de Física Aplicada, Universitat Politècnica de Catalunya, Spain; and ‡Department of Mathematics, University of Central Florida and Purdue University*

E-mail: lopez@math.la.asu.edu; marques@fa.upc.es; shen@math.purdue.edu

Received February 9, 2001; revised December 10, 2001

An efficient and accurate numerical scheme is presented for the three-dimensional Navier–Stokes equations in primitive variables in a cylinder. The scheme is based on a spectral-Galerkin approximation for the space variables and a second-order projection scheme for time. The new spectral-projection scheme is implemented to simulate unsteady incompressible flows in a cylinder. © 2002 Elsevier Science (USA)

Key Words: spectral-Galerkin method; projection method; Navier–Stokes; rotating waves.

1. INTRODUCTION

There are many fundamental issues in fluid dynamics that can be effectively addressed by the study of flows in cylindrical containers (e.g., symmetry breaking, transition to complex dynamics). The attraction of such a flow geometry is that, although the system is fully three dimensional, the invariance of the equations and boundary conditions to arbitrary rotations in azimuth (the $SO(2)$ symmetry) naturally provides a periodic direction (the azimuthal direction, θ) which can be efficiently exploited in the solution scheme.

In Lopez and Shen [13], we presented an efficient and accurate spectral scheme for the axisymmetric Navier–Stokes equations in cylindrical geometries. There, due to the imposed symmetry, the problem reduced to a set of two-dimensional partial differential equations. In this paper, we do not impose any symmetry on the solutions, and generalize the aforementioned solver to the fully three-dimensional case.

Several distinct approaches have been formulated to solve the three-dimensional Navier–Stokes equations in cylindrical geometries. Here, we restrict our attention to finite, enclosed containers, and so the axial direction is not periodic. A popular approach is to use finite difference or finite volume spatial discretization for such problems (e.g., [20, 26, 30]). The pole singularity at the axis, however, requires special treatment; this may be a reformulation of the governing equations or the use of staggered grid strategies and specifically tailored derivatives at the axis. If a mapping on a curvilinear Cartesian-type grid is employed, the symmetry of the system is destroyed, which can lead to qualitatively different dynamics. The use of cylindrical polars within the finite difference/volume formulations leads to excessive grid clustering about $r = 0$, which leads to an ill-conditioned system with severe time-step restrictions, and often *ad hoc* smoothing is employed. Finite difference/volume methods are generally less accurate than spectral methods, and when used for large Reynolds number flows in three dimensions, the required number of grid points becomes excessive for a practical implementation. Tuckerman [29] introduced the influence matrix method, within a pseudospectral Galerkin scheme, for cylindrical geometries with only one periodic direction (θ) that exactly enforced incompressibility. However, this proved to be impractical for three-dimensional Navier–Stokes at moderate Reynolds numbers due to excessive memory requirements. Incompressibility may also be imposed by decomposing the velocity into toroidal and poloidal potentials [14], and such a formulation has recently been implemented for three-dimensional Navier–Stokes in an enclosed cylinder [22]. This method is attractive because pressure is not explicit in the governing equations, but the order of the equations is higher leading to poor conditioning, and there is coupling between the potentials through the boundary conditions. A spectral element method has also been used for this class of problems [2], although the simple cylindrical geometry does not require the added sophistication of the method.

Here we present the formulation, and sample computations at moderate Reynolds numbers, of the generalization of the spectral-projection scheme in Lopez and Shen [13] to three dimensions.

2. THREE-DIMENSIONAL NAVIER–STOKES EQUATIONS IN CYLINDRICAL COORDINATES

We consider an incompressible flow confined in a cylinder (the flow between two concentric cylinders can be handled with a similar technique, and is in fact easier to deal with because of the absence of the coordinate singularity), i.e., the domain in cylindrical coordinates (r, θ, z) is

$$\Omega = \{0 \leq r < R, 0 \leq \theta < 2\pi, 0 < z < H\}.$$

The equations governing the flow are Navier–Stokes, together with initial and boundary conditions. We denote the velocity vector and pressure, respectively, by $\mathbf{u} = (u, v, w)^T$ and p . Then, the Navier–Stokes equations in velocity-pressure formulation written in cylindrical coordinates are

$$\partial_t u - \frac{1}{Re} \left(\nabla^2 u - \frac{1}{r^2} u + \frac{2}{r^2} \partial_\theta v \right) + \partial_r p + \text{adv}_r = f_r, \quad (1)$$

$$\partial_t v - \frac{1}{Re} \left(\nabla^2 v - \frac{1}{r^2} v - \frac{2}{r^2} \partial_\theta u \right) + \partial_\theta p + \text{adv}_\theta = f_\theta, \quad (2)$$

$$\partial_t w - \frac{1}{Re} \nabla^2 w + \partial_z p + \text{adv}_z = f_z, \quad (3)$$

$$\frac{1}{r} \partial_r(ru) + \frac{1}{r} \partial_\theta v + \partial_z w = 0, \quad (4)$$

where

$$\nabla^2 = \partial_r^2 + \frac{1}{r} \partial_r + \frac{1}{r^2} \partial_\theta^2 + \partial_z^2 \quad (5)$$

is the Laplace operator in cylindrical coordinates,

$$\text{adv}_r = u \partial_r u + \frac{1}{r} v \partial_\theta u + w \partial_z u - \frac{1}{r} v^2,$$

$$\text{adv}_\theta = u \partial_r v + \frac{1}{r} v \partial_\theta v + w \partial_z v - \frac{1}{r} uv, \quad (6)$$

$$\text{adv}_z = u \partial_r w + \frac{1}{r} v \partial_\theta w + w \partial_z w,$$

and $(f_r, f_\theta, f_z)^T$ is an externally imposed body force. The equations are to be completed with admissible initial and boundary conditions.

Note that in addition to the nonlinear coupling, the velocity components (u, v) are also coupled in the linear viscous terms in this case. Following Orszag and Patera [19], we introduce a new set of complex functions

$$u_+ = u + iv, \quad u_- = u - iv, \quad (7)$$

where i is the unit imaginary number. Note that

$$u = \frac{1}{2}(u_+ + u_-), \quad v = \frac{1}{2i}(u_+ - u_-). \quad (8)$$

The Navier–Stokes equations (1)–(4) under the new unknown functions (u_+, u_-, w, p) are

$$\partial_t u_+ - \frac{1}{Re} \left(\nabla^2 - \frac{1}{r^2} + \frac{2i}{r^2} \partial_\theta \right) u_+ + \left(\partial_r + \frac{i}{r} \partial_\theta \right) p + \text{adv}_+ = f_+, \quad (9)$$

$$\partial_t u_- - \frac{1}{Re} \left(\nabla^2 - \frac{1}{r^2} - \frac{2i}{r^2} \partial_\theta \right) u_- + \left(\partial_r - \frac{i}{r} \partial_\theta \right) p + \text{adv}_- = f_-, \quad (10)$$

$$w_t - \frac{1}{Re} \nabla^2 w + \partial_z p + \text{adv}_z = f_z, \quad (11)$$

$$\left(\partial_r + \frac{1}{r} \right) \frac{u_+ + u_-}{2} + \frac{1}{ir} \partial_\theta \frac{u_+ - u_-}{2} + \partial_z w = 0, \quad (12)$$

where we have denoted

$$\text{adv}_\pm = \text{adv}_r \pm i \text{adv}_\theta, \quad p f_\pm = f_r \pm i f_\theta. \quad (13)$$

Now, u_+ and u_- in the linear viscous terms in the formulation (9)–(12) are decoupled, just as in the Cartesian case.

2.1. Dimension Reduction

Since all the relevant functions are periodic in the azimuthal direction θ , we set

$$\begin{aligned} (u_{\pm}, w, p) &= \sum_{m=-\infty}^{+\infty} (u_{\pm,m}, w_m, p_m) e^{im\theta}, \\ (\text{adv}_{\pm}, \text{adv}_z, f_{\pm}, f_z) &= \sum_{m=-\infty}^{+\infty} (\text{adv}_{\pm,m}, \text{adv}_{z,m}, f_{\pm,m}, f_{z,m}) e^{im\theta}. \end{aligned} \quad (14)$$

By definition, we have $\bar{u}_{+,-m} = u_{-,m}$ (where the overbar denotes complex conjugate) for all m . Moreover, w and p are real functions so that $\bar{w}_m = w_{-m}$ and $\bar{p}_m = p_{-m}$. Therefore, we only have to compute $u_{\pm,m}$, w_m and p_m for $m \geq 0$. Furthermore, we have $u_{+,0} = \bar{u}_{-,0}$. Hence, for $m=0$, we only need to compute $\Re(u_{+,0})$ and $\Im(u_{+,0})$, which are the real and imaginary parts of $u_{+,0}$, respectively.

Now, substituting the above expansions into (9)–(12) and collecting the terms for each mode m , we find that $(u_{\pm,m}(r, z), w_m(r, z), p_m(r, z))$ satisfy the following equations with $(r, z) \in \mathcal{D} := \{(r, z) : 0 \leq r < R, 0 < z < H\}$:

(i) for $m > 0$:

$$\begin{aligned} \left(\partial_t - \frac{1}{Re} \nabla_{m+1}^2 \right) u_{+,m} + \partial_{-m,r} p_m + \text{adv}_{+,m} &= f_{+,m}, \\ \left(\partial_t - \frac{1}{Re} \nabla_{m-1}^2 \right) u_{-,m} + \partial_{m,r} p_m + \text{adv}_{-,m} &= f_{-,m}, \\ \left(\partial_t - \frac{1}{Re} \nabla_m^2 \right) w_m + \partial_z p_m + \text{adv}_{z,m} &= f_{z,m}, \\ \frac{1}{2} (\partial_{m+1,r} u_{+,m} + \partial_{-m+1,r} u_{-,m}) + \partial_z w_m &= 0, \end{aligned} \quad (15)$$

(ii) for $m = 0$:

$$\begin{aligned} \left(\partial_t - \frac{1}{Re} \nabla_1^2 \right) \Re(u_{+,0}) + \partial_r p_0 + \Re(\text{adv}_{+,0}) &= \Re(f_{+,0}), \\ \left(\partial_t - \frac{1}{Re} \nabla_1^2 \right) \Im(u_{+,0}) + \Im(\text{adv}_{+,0}) &= \Im(f_{+,0}), \\ \left(\partial_t - \frac{1}{Re} \nabla_0^2 \right) w_0 + \partial_z p_0 + \text{adv}_{z,0} &= f_{z,0}, \\ \partial_{1,r} \Re(u_{+,0}) + \partial_z w_0 &= 0, \end{aligned} \quad (16)$$

where

$$\nabla_k^2 = \frac{1}{r} \partial_r (r \partial_r) - \frac{k^2}{r^2} + \partial_z^2, \quad \text{and} \quad \partial_{k,r} = \partial_r + \frac{k}{r}. \quad (17)$$

The above equations are to be completed with the initial and boundary conditions stemming from those of (1)–(4) and from suitable pole conditions to be described below.

2.2. Pole Conditions

The polar transformation is singular at $r = 0$. Hence, for a function in Cartesian coordinates $U(x, y, z)$ to have certain regularity at the pole (i.e., $x = y = 0$), the function $u(r, \theta, z) = U(r \cos \theta, r \sin \theta, z)$ in polar coordinates needs to satisfy corresponding pole conditions at $r = 0$. Since we are interested in the approximation of the usual variational formulation of the Navier–Stokes equations, we shall use the term *essential pole conditions* to denote those which are necessary for the well-posedness of the variational formulation of the Navier–Stokes equations. All other pole conditions, which will imply more regularity of the solutions at the poles, are *natural pole conditions*; see [3, 23]. Just as the Neumann boundary condition in a variational formulation should be treated *naturally*, i.e., built-in the weak variational formulation, rather than imposed *essentially*, these *natural pole conditions* should also be treated *naturally* with a suitable weak variational formulation, cf. (20)–(21).

Different aspects of appropriate pole conditions in the context of spectral methods have been discussed by numerous authors, cf. [9, 17, 21, 29]. Our discussion below is focused on determining the *essential* and *natural* pole conditions for the Navier–Stokes equations. The *essential pole conditions* can be determined as follows.

To simplify the presentation, we introduce the following notation for $m > 0$ as

$$\Delta_m = \begin{pmatrix} \nabla_{m+1}^2 & 0 & 0 \\ 0 & \nabla_{m-1}^2 & 0 \\ 0 & 0 & \nabla_m^2 \end{pmatrix}, \quad \nabla_m = \begin{pmatrix} \partial_{-m,r} \\ \partial_{m,r} \\ \partial_z \end{pmatrix},$$

$$\mathbf{u}_m = (u_{+,m}, u_{-,m}, w_m)^T,$$

$$\nabla_m \cdot \mathbf{u}_m = \frac{1}{2}(\partial_{m+1,r}u_{+,m} + \partial_{-m+1,r}u_{-,m}) + \partial_z w_m,$$

and rewrite (15) in vector form ($m > 0$) as

$$\partial_t \mathbf{u}_m - \frac{1}{Re} \Delta_m \mathbf{u}_m + \nabla_m p_m = \mathbf{N}_m(\mathbf{u}, \mathbf{f}),$$

$$\nabla_m \cdot \mathbf{u}_m = 0, \tag{18}$$

where $\mathbf{N}_m(\mathbf{u}, \mathbf{f})$ represents the nonlinear and forcing terms in (15).

Similarly, let $\mathbf{N}_0(\mathbf{u}, \mathbf{f})$ represent the nonlinear and forcing terms in (16) and set

$$\Delta_0 = \begin{pmatrix} \nabla_1^2 & 0 & 0 \\ 0 & \nabla_1^2 & 0 \\ 0 & 0 & \nabla_0^2 \end{pmatrix}, \quad \nabla_0 = \begin{pmatrix} \partial_r \\ 0 \\ \partial_z \end{pmatrix},$$

$$\mathbf{u}_0 = (\Re(u_{+,0}), \Im(u_{+,0}), w_0)^T,$$

$$\nabla_0 \cdot \mathbf{u}_0 = \partial_{1,r} \Re(u_{+,0}) + \partial_z w_0.$$

So, in vector form, (16) becomes

$$\partial_t \mathbf{u}_0 - \frac{1}{Re} \Delta_0 \mathbf{u}_0 + \nabla_0 p_0 = \mathbf{N}_0(\mathbf{u}, \mathbf{f}),$$

$$\nabla_0 \cdot \mathbf{u}_0 = 0. \tag{19}$$

The bilinear form corresponding to $-\Delta_m$ with $m > 0$, associated with the variational formulation of (18), is

$$\begin{aligned} a_m(\mathbf{u}_m, \mathbf{v}_m) &:= (r \partial_r u_{+,m}, \partial_r v_{+,m}) + (m+1) \left(\frac{1}{r} u_{+,m}, v_{+,m} \right) + (\partial_z u_{+,m}, \partial_z v_{+,m}) \\ &\quad + (r \partial_r u_{-,m}, \partial_r v_{-,m}) + (m-1) \left(\frac{1}{r} u_{-,m}, v_{-,m} \right) + (\partial_z u_{-,m}, \partial_z v_{-,m}) \\ &\quad + (r \partial_r w_m, \partial_r w_m) + (\partial_z w_m, \partial_z w_m), \end{aligned} \quad (20)$$

where $(f, g) := \int_0^R dr \int_0^{2\pi} d\theta \int_0^H f \bar{g} dz$ (R and H are the radius and the height of the cylinder, respectively). The bilinear form $a_m(\mathbf{u}_m, \mathbf{v}_m)$ is simply the inner product of $-\Delta_m \mathbf{u}_m$ with $r \mathbf{v}_m$ (r is the Jacobian of the polar transform) after integrating by parts. Similarly, the bilinear form corresponding to $-\Delta_0$, associated with the variational formulation of (19), is

$$\begin{aligned} a_0(\mathbf{u}_0, \mathbf{v}_0) &:= (r \partial_r \Re(u_{+,0}), \partial_r \Re(v_{+,0})) + \left(\frac{1}{r} \Re(u_{+,0}), \Re(v_{+,0}) \right) + (\partial_z \Re(u_{+,0}), \partial_z \Re(v_{+,0})) \\ &\quad + (r \partial_r \Im(u_{+,0}), \partial_r \Im(v_{+,0})) + \left(\frac{1}{r} \Im(u_{+,0}), \Im(v_{+,0}) \right) \\ &\quad + (\partial_z \Im(u_{+,0}), \partial_z \Im(v_{+,0})) + (r \partial_r w_0, \partial_r w_0) + (\partial_z w_0, \partial_z w_0). \end{aligned} \quad (21)$$

Thus, the *essential* pole conditions for \mathbf{u}_m (and for the test function \mathbf{v}_m) are those which ensure that all the integrals in the bilinear form $a_m(\mathbf{u}_m, \mathbf{v}_m)$ are finite. Specifically, on the axis ($r = 0$), the following pole conditions are *essential*:

$$\begin{aligned} m > 1: & \quad u_{+,m} = u_{-,m} = w_m = 0, \\ m = 1: & \quad u_{+,1} = w_1 = 0, \\ m = 0: & \quad u_{+,0} = 0. \end{aligned} \quad (22)$$

The *essential* pole condition for the pressure is determined by requiring the pressure to be single-valued at the pole, i.e., $\frac{\partial p}{\partial \theta}|_{r=0} = 0$, which implies that

$$p_m|_{r=0} = 0, \quad m \neq 0. \quad (23)$$

2.3. Regularity Conditions on the Axis

The *essential* pole conditions (22)–(23) will ensure the well-posedness of equations (15)–(16) and the regularity (in the polar coordinates) of their solutions in appropriate weighted Sobolev spaces; see [1] for related theoretical aspects. Thus, the *essential* pole conditions are sufficient for the purpose of numerical approximations, as demonstrated in Shen [25] for elliptic equations and in Lopez and Shen [13] for axisymmetric Navier–Stokes equations. Nevertheless, these *essential* pole conditions will not ensure the smoothness of the solutions at the pole in Cartesian coordinates. For the readers' convenience, we present below a simple derivation of regularity conditions on the axis.

The regularity conditions on the axis are a consequence of the singularity of the cylindrical polar coordinates at $r = 0$: the value of any physical quantity at $r = 0$, $\theta \in [0, 2\pi)$ must be unique. For the sake of simplicity of exposition, we shall drop the dependence on z in this

section since it has no effect on the singularity at the axis. We write

$$\begin{aligned} \mathbf{u} &= u(r, \theta)\hat{\mathbf{r}} + v(r, \theta)\hat{\boldsymbol{\theta}} + w(r, \theta)\hat{\mathbf{k}} \\ &= u_x(x, y)\hat{\mathbf{i}} + u_y(x, y)\hat{\mathbf{j}} + u_z(x, y)\hat{\mathbf{k}}, \end{aligned} \tag{24}$$

where $(\hat{\mathbf{i}}, \hat{\mathbf{j}}, \hat{\mathbf{k}})$ and $(\hat{\mathbf{r}}, \hat{\boldsymbol{\theta}}, \hat{\mathbf{k}})$ are, respectively, the unit vectors in Cartesian and polar coordinates. We recall that

$$\hat{\mathbf{r}} = \cos \theta \hat{\mathbf{i}} + \sin \theta \hat{\mathbf{j}}, \quad \hat{\boldsymbol{\theta}} = -\sin \theta \hat{\mathbf{i}} + \cos \theta \hat{\mathbf{j}}, \tag{25}$$

and a simple computation leads to

$$u_{\pm}(r, \theta) = u(r, \theta) \pm i v(r, \theta) = e^{\mp i \theta} (u_x(x, y) \pm i u_y(x, y)). \tag{26}$$

Assuming analyticity of the function \mathbf{u} in Cartesian coordinates, the regularity conditions in polar coordinates are now derived.

Let us first consider the axial component of velocity, w . Introducing the complex variable $\zeta = r e^{i \theta}$, we have $x = (\zeta + \bar{\zeta})/2$, $y = -i(\zeta - \bar{\zeta})/2$, and

$$w(r, \theta) = u_z(x, y) = u_z((\zeta + \bar{\zeta})/2, -i(\zeta - \bar{\zeta})/2) = \eta(\zeta, \bar{\zeta}).$$

Since $u_z(x, y)$ is analytic and the coordinate change $(x, y) \leftrightarrow (\zeta, \bar{\zeta})$ is linear, the function $\eta(\zeta, \bar{\zeta})$ is analytic and can be expanded as a Taylor series:

$$\eta(\zeta, \bar{\zeta}) = \sum_{p,q=0}^{+\infty} \eta_{p,q} \zeta^p \bar{\zeta}^q.$$

Using the Taylor expansion of $\eta(\zeta, \bar{\zeta})$ in the expression of $w_m(r)$, the m th Fourier mode of w in (14), we get for $m \geq 0$:

$$\begin{aligned} w_m(r) &= \frac{1}{2\pi} \int_0^{2\pi} \eta(\zeta, \bar{\zeta}) e^{-im\theta} d\theta = \sum_{p,q=0}^{+\infty} \eta_{p,q} r^{p+q} \frac{1}{2\pi} \int_0^{2\pi} e^{i(p-q-m)\theta} d\theta \\ &= \sum_{p-q=m; p,q=0}^{+\infty} \eta_{p,q} r^{p+q} = r^m \sum_{q=0}^{+\infty} \eta_{q+m,q} r^{2q}. \end{aligned} \tag{27}$$

This expression gives the regularity conditions for w_m on the axis.

The corresponding conditions for $u_{\pm,m}$ can be obtained analogously. More precisely, from (26), we can write

$$u_{\pm}(r, \theta) = e^{\mp i \theta} \eta_{\pm}(\zeta, \bar{\zeta}), \tag{28}$$

where $\eta_{\pm}(\zeta, \bar{\zeta})$ are analytic functions with Taylor expansions

$$\eta_{\pm}(\zeta, \bar{\zeta}) = \sum_{p,q=0}^{+\infty} \eta_{\pm,p,q} \zeta^p \bar{\zeta}^q.$$

The m th Fourier mode of $u_{\pm}(r, \theta)$, expanded as shown in (14), can now be expressed as

$$\begin{aligned} u_{\pm, m}(r) &= \frac{1}{2\pi} \int_0^{2\pi} \eta_{\pm}(\zeta, \bar{\zeta}) e^{-i(m\pm 1)\theta} d\theta \\ &= \sum_{p-q=m\pm 1; p, q=0}^{+\infty} \eta_{\pm, p, q} r^{p+q} = r^{m\pm 1} \sum_{q=0}^{+\infty} \eta_{\pm, q, m\pm 1+q} r^{2q}. \end{aligned} \quad (29)$$

This expression gives the regularity conditions on the axis for $u_{+, m}$ with $m \geq 0$ and $u_{-, m}$ with $m \geq 1$ (note that $\bar{u}_{-, 0} = u_{+, 0}$).

The regularity conditions (27) and (29) can be imposed using expansions in appropriate special functions; e.g., [4, 17]. For high m -values, these regularity conditions produce ill-conditioned matrices, and are often imposed only for the first few values of m ; e.g., see [21].

The regularity conditions on the axis can be grouped into two parts. First, the factors r^m and $r^{m\pm 1}$ appearing in the expressions of $u_{\pm, m}$ (29) and w_m (27) give, in addition to the *essential* pole conditions (22), a set of *natural* pole conditions on the axis

$$\begin{aligned} \partial_r^k u_{+, m} &= 0, & k = 1, \dots, m; m \geq 1, \\ \partial_r^k u_{-, m} &= 0, & k = 1, \dots, m - 2; m \geq 3, \\ \partial_r^k w_m &= 0, & k = 1, \dots, m - 1; m \geq 2. \end{aligned} \quad (30)$$

Second, the dependence on r^2 in $u_{\pm, m}$ and w_m gives the following *parity* conditions on the axis:

$$u_{\pm, m} \text{ has the same parity as } m + 1; \quad w_m \text{ has the same parity as } m. \quad (31)$$

Note that the pole condition $\partial_r w_0|_{r=0} = 0$ used in Lopez and Shen [13], and by others for axisymmetric problems, is not a part of the natural pole conditions. Instead, it is a consequence of the parity condition satisfied by w_0 .

In our approach, only the essential pole conditions (22) are imposed. This is the minimal set of regularity conditions on the axis necessary for the well-posedness of the variational formulation of the Navier–Stokes equations; see Bernardi *et al.* [1] for a complete theoretical analysis.

3. DISCRETIZATION BY A SPECTRAL-PROJECTION SCHEME

We consider the Navier–Stokes equations (9)–(12) subject to an initial condition $\mathbf{u}|_{t=0} = \mathbf{u}_0$ and a Dirichlet boundary condition for velocity

$$\mathbf{u}(t)|_{\partial\Omega} = \mathbf{g}(t)|_{\partial\Omega}. \quad (32)$$

Other admissible boundary conditions can be treated similarly.

3.1. Time Discretization: A Second-Order Projection Method

As in Lopez and Shen [13], the equations (18)–(19) with the pole conditions (22) and the boundary conditions (32) are discretized in time by a second-order projection scheme.

More precisely, we use an improved version of the second-order projection scheme, which we shall refer to as the second-order projection scheme with divergence correction.

Let $\Gamma_1 = \{r = 0 : 0 < z < H\}$ and $\Gamma_2 = \partial\mathcal{D} \setminus \Gamma_1$. Using the identity

$$\nabla_m \cdot \nabla_m = \frac{1}{r} \partial_r (r \partial_r) - \frac{m^2}{r^2} + \partial_z^2 = \nabla_m^2,$$

the second-order BDF (backward difference formula) projection scheme with divergence correction is as follows:

In the first step, we solve for an intermediate velocity $\tilde{\mathbf{u}}_m^{k+1} (m \geq 0)$ from

$$\frac{1}{2\delta t} (3\tilde{\mathbf{u}}_m^{k+1} - 4\mathbf{u}_m^k + \mathbf{u}_m^{k-1}) - \frac{1}{Re} \Delta_m \tilde{\mathbf{u}}_m^{k+1} = -\nabla_m p_m^k - 2\mathbf{N}_m^k + \mathbf{N}_m^{k-1}, \tag{33}$$

with the boundary conditions

$$\tilde{\mathbf{u}}_m^{k+1} |_{\Gamma_2} = \mathbf{g}_m^{k+1}, \tag{34}$$

and the essential pole conditions (22) on the axis Γ_1 :

$$\begin{aligned} m > 1: \quad & \tilde{u}_{+,m}^{k+1} = \tilde{u}_{-,m}^{k+1} = \tilde{w}_m^{k+1} = 0, \\ m = 1: \quad & \tilde{u}_{+,1}^{k+1} = \tilde{w}_1^{k+1} = 0, \\ m = 0: \quad & \tilde{u}_{+,0}^{k+1} = 0. \end{aligned} \tag{35}$$

In the above, $\mathbf{N}_m^j = \mathbf{N}_m(\mathbf{u}, \mathbf{f})|_{t=j \delta t}$ and \mathbf{g}_m^j is the m th Fourier mode of $\mathbf{g}|_{t=j \delta t}$.

In the second step,¹ we solve for $\phi_m^{k+1} (m \geq 0)$ from

$$-\nabla_m^2 \phi_m^{k+1} = -\frac{3}{2\delta t} \nabla_m \cdot \tilde{\mathbf{u}}_m^{k+1}, \tag{36}$$

with the boundary conditions (cf. (23))

$$\frac{\partial}{\partial \mathbf{n}} \phi_0^{k+1} |_{\partial\mathcal{D}} = 0; \quad \frac{\partial}{\partial \mathbf{n}} \phi_m^{k+1} |_{\Gamma_2} = 0, \quad \phi_m^{k+1} |_{\Gamma_1} = 0 \quad (m \geq 1), \tag{37}$$

where \mathbf{n} is the outward normal. Then, we set

$$\begin{aligned} p_m^{k+1} &= \phi_m^{k+1} + p_m^k - \frac{1}{Re} \nabla_m \cdot \tilde{\mathbf{u}}_m^{k+1}, \\ \mathbf{u}_m^{k+1} &= \tilde{\mathbf{u}}_m^{k+1} - \frac{2\delta t}{3} \nabla_m \phi_m^{k+1}. \end{aligned} \tag{38}$$

Thus, at each time step ($t = (k + 1)\delta t, k = 0, 1, \dots$) and for each nonnegative Fourier mode m , we need to solve a Poisson-type equation (33) for each of the velocity components $\tilde{\mathbf{u}}_m^{k+1}$, and a Poisson equation (36) for ϕ_m^{k+1} .

Note that the difference between the above scheme and the one used in Lopez and Shen [13] is that in the second step, a divergence correction term is introduced (see the first

¹ Note that there were some misprints in Lopez and Shen [13]; in fact, $\frac{1}{2\delta t}$ in (2.3) and (2.4) should be $\frac{3}{2\delta t}$, and accordingly, $2\delta t$ in (2.5) should be $\frac{2\delta t}{3}$.

equation in (38)). The immediate consequence of this divergence correction term is that the pressure approximation p_m^k now satisfies a consistent Neumann boundary condition, instead of the artificial homogeneous Neumann boundary condition in the absence of the divergence correction term. While the scheme with divergence correction does not improve the formal accuracy of the velocity, it does lead to substantially more accurate pressure approximations; see, for instance, Timmermans, Mineev and Van De Vosse [28] and Guermond and Shen [7].

3.2. Spatial Discretization: Spectral-Galerkin Methods

From the above projection scheme, we find that each member of $(\tilde{u}_{\pm,m}^k, \tilde{w}_m^k, \phi_m^k)$, $m \geq 0$ and $k \geq 1$, denoted by a generic function v , satisfies a Poisson-type equation of the form

$$\alpha v - \nabla_j^2 v = h, \quad \text{in } \mathcal{D}, \tag{39}$$

where α is a given nonnegative constant ($\alpha = 0$ for ϕ_0^k), h is a given function, and j is a nonnegative number ($j = 0$ only for u_{-1}^k, w_0^k and ϕ_0^k). This Poisson-type equation is supplemented with one of the four boundary conditions as follows:

1. $v|_{\Gamma_2} = g, v|_{\Gamma_1} = 0$ (for all $u_{\pm,m}^k$ and w_m^k , except u_{-1}^k and w_0^k).
2. $v|_{\Gamma_2} = g$ (for u_{-1}^k and w_0^k).
3. $\frac{\partial v}{\partial \mathbf{n}}|_{\partial \mathcal{D}} = 0$ (for ϕ_0^k).
4. $\frac{\partial}{\partial \mathbf{n}} \phi_m^{k+1}|_{\Gamma_2} = 0, \phi_m^{k+1}|_{\Gamma_1} = 0$ for ϕ_m^k with $m \geq 1$.

These Poisson-type equations are solved by using the fast spectral-Galerkin methods developed in Shen [23] and Shen [25]. For the readers' convenience, we provide some details below.

Since the nonhomogeneous Dirichlet boundary conditions can be easily lifted in a rectangular domain (see Shen, [23], for a detailed implementation procedure), we can assume, for the sake of simplicity, that $g = 0$ in the above. In addition to the Sobolev space $H^1(\mathcal{D})$ and $H_0^1(\mathcal{D})$, we denote also

$$H_0^1(\mathcal{D}) := \{u \in H^1(\mathcal{D}) : u|_{\Gamma_2} = 0\}. \tag{40}$$

Thus, the variational formulation for the Poisson-type equation, obtained by taking the inner product of (39) with $r w$ (where r is the Jacobian of the polar transformation) and integrating by parts, with one of the three boundary conditions is: Find $v \in X$ such that

$$\alpha(rv, w) + (r\partial_r v, \partial_r w) + k^2 \left(\frac{1}{r} v, w \right) = (rh, w), \quad \forall w \in X, \tag{41}$$

where $X = H_0^1(\mathcal{D})$ for the first boundary condition; $X = H_0^1(\mathcal{D})$ for the second; $X = H^1(\mathcal{D})$ for the third (for ϕ_0^k , $X = H^1(\mathcal{D}) \setminus \mathbb{R}$ should be used to fix the free-constant in the pressure); and $(v, w) = \int_0^R dr \int_0^H v w dz$.

Let us denote by P_N the set of polynomials of degree less than or equal to N and $P_{NM} = P_N \times P_M$. Let $X_{NM} \subset P_{NM}$ be an appropriate approximation space for X . The Legendre–Galerkin method for (41) is to find v_{NM} in X_{NM} such that

$$\alpha(rv_{NM}, w) + (r\partial_r v_{NM}, \partial_r w) + k^2 \left(\frac{1}{r} v_{NM}, w \right) = (rI_{NM}h, w), \quad \forall w \in X_{NM}, \tag{42}$$

where $I_{NM} : C(\mathcal{D}) \rightarrow P_{NM}$ is the polynomial interpolation operator based on the Gauss–Lobatto points.

As demonstrated in Shen [23] and Shen [25], a suitable choice of basis functions for X_{NM} will lead to a sparse linear system which can be efficiently solved. More precisely, let $L_j(x)$ be the j th degree Legendre polynomial, and set

$$\begin{aligned} \phi_j(x) &= L_j(x) - L_{j+2}(x), \\ \psi_j(x) &= L_j(x) + L_{j+1}(x), \\ \gamma_j(x) &= L_j(x) - \frac{j(j+1)}{(j+2)(j+3)}L_{j+2}(x), \\ \xi_j(x) &= L_j(x) + \frac{2j+3}{(j+2)^2}L_{j+1}(x) + \left(\frac{2j+3}{(j+2)^2} - 1\right)L_{j+2}(x). \end{aligned} \tag{43}$$

One can easily check by using the properties of Legendre polynomials that

$$\phi_j(\pm 1) = 0; \quad \psi_j(-1) = 0; \quad \partial_x \gamma_j(\pm 1) = 0; \quad \xi_j(-1) = 0, \quad \partial_x \xi_j(1) = 0.$$

These functions are used as basis functions for X_{NM} . Let $(\hat{r}, \hat{z}) = (\frac{2r-R}{R}, \frac{2z-H}{H})$ so that $(r, z) \in \mathcal{D}$ is mapped to $(\hat{r}, \hat{z}) \in \hat{\mathcal{D}} := (-1, 1)^2$. Then,

- for the first boundary condition, $X_{NM} = P_{NM} \cap H_0^1(\mathcal{D})$ so that

$$X_{NM} = \{\phi_i(\hat{r})\phi_j(\hat{z}) : i = 0, 1, \dots, N - 2, j = 0, 1, \dots, M - 2\};$$

- for the second boundary condition, $X_{NM} = P_{NM} \cap H_0^1(\mathcal{D})$ so that

$$X_{NM} = \{\psi_i(\hat{r})\phi_j(\hat{z}) : i = 0, 1, \dots, N - 2, j = 0, 1, \dots, M - 2\};$$

- for the third boundary condition, two options are available:
 1. If the pressure is a physical quantity of interest, we should use

$$X_{NM} = P_{N-2, M-2} = \text{span}\{L_i(\hat{r})L_j(\hat{z}) : i = 0, 1, \dots, N - 2, j = 0, 1, \dots, M - 2\}.$$

In this case, the inf–sup condition between the velocity and pressure approximation spaces is verified so the pressure approximation will converge to the exact pressure.

2. If the pressure is not a physical quantity of interest (which is the case for the application in this paper), we can set $X_{NM} = \{v \in P_{NM} : \frac{\partial v}{\partial \mathbf{n}}|_{\partial \mathcal{D}} = 0\} \setminus \mathbb{R}$ so that

$$X_{NM} = \{\gamma_i(\hat{r})\gamma_j(\hat{z}) : i = 0, 1, \dots, N - 2, j = 0, 1, \dots, M - 2\} \setminus \mathbb{R}.$$

In this case, the pressure approximation may contain spurious modes. However, it will not affect the accuracy of the velocity approximation, and the resulting linear system can be solved much more efficiently [23].

- For the fourth boundary condition, the treatment is similar to the third boundary condition with $\gamma_i(\hat{r})$ replaced by $\xi_i(\hat{r})$.

One can check that, using these basis functions, the stiffness and mass matrices associated with (42) are all sparse, and as demonstrated in Shen [23] and Shen [25], the resulting linear systems can be solved efficiently by using a matrix decomposition method. We refer to

Shen [23, 25] and Lopez and Shen [13] for more details on spectral-Galerkin algorithms for these Poisson type equations.

We end this section with a number of remarks.

- The nonlinear terms are evaluated at the collocation points using the so-called transform (i.e., pseudospectral) method; e.g., [4].
- The cost of solving each Poisson-type equation using the Legendre–Galerkin method is $O(NM \min(N, M))$ [23, 25]. If L Fourier modes are used in the azimuthal direction and fast Fourier transforms (FFTs) are used, the total cost of the spectral-projection scheme at each time step is of the order $NML \min(N, M) \log L$. This operational count can be further reduced to $NML \log(NML)$ by using the optimized Chebyshev–Legendre Galerkin method in the (r, z) directions [24, 25]. Hence, with the same number of unknowns, the cost of our spectral solvers are very competitive with those based on finite-difference or finite-element discretizations, while offering much better resolution properties and accuracy.
- We refer to Lopez and Shen [13] for a discussion of the time-step constraint of this spectral-projection scheme.
- The application of this spectral-projection scheme to flow between two concentric cylinders is straightforward.

4. NUMERICAL RESULTS

Most test problems for convergence with the pole condition are restricted to (r, θ) -planes and consist of linear scalar equations, e.g., finding roots of Bessel functions on the disk and solving scalar Poisson equations. The pole conditions for vector problems are different and have not usually been treated. Our main motivation for developing the present scheme is the solution of three-dimensional Navier–Stokes equations, and as such, the vector problem is prevalent.

Having performed a typical test procedure, where one chooses an exact time-dependent solution and uses the proposed scheme to approximate it, which has confirmed the overall correctness of the code, we now consider a physically relevant three-dimensional test problem of the flow in a cylinder of height H and radius R , filled with an incompressible fluid of kinematic viscosity ν , driven by the rotation of one endwall at Ω rad/s. This single problem provides stringent tests of all aspects of our code. This problem has been widely studied; see, e.g., [5, 6, 10–12, 27], mainly because of the existence over a wide range of the governing parameters, $Re = \Omega R^2/\nu$ and $\Lambda = H/R$, of flow states with recirculation zones in the central vortex, known as vortex breakdown bubbles. In spite of numerous numerical and experimental studies, considerable controversy with fundamental aspects of this flow continues, particularly with regard to symmetry breaking.

The boundary conditions on Γ_2 for $(u_{\pm, m}, w_m)$ for this problem are all zero except that $v_0|_{z=0} = r$. Note that this boundary condition is discontinuous at the corner $(r, z) = (R, 0)$. This discontinuity is treated by using the procedure in Lopez and Shen [13], which produces mesh independent approximations to the discontinuous boundary condition to within any prescribed accuracy. All results presented below are obtained with $64 \times 64 \times 16$ modes.

The axisymmetric version of the present code [13] has been instrumental in obtaining detailed knowledge of the axisymmetric basic state. Recent developments, e.g., [2, 6, 15, 16], indicate that nonaxisymmetric bifurcations play an important role in extensive regions of parameter space. The linear stability analysis of Gelfgat *et al.* [8] indicates that the primary bifurcation is nonaxisymmetric in the ranges $\Lambda < 1.6$ and $\Lambda > 2.8$, and in these

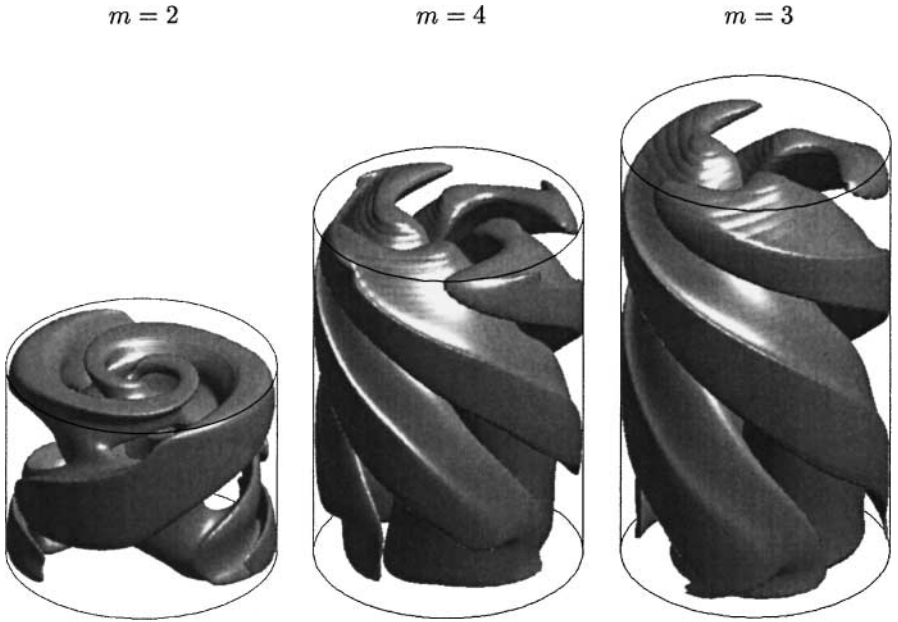


FIG. 1. Three-dimensional perspective of w_p (isosurface close to the zero-level) for pure rotating wave solutions corresponding to (Re, Λ) parameter values $(2750, 1.58)$ for the $m = 2$ RW, $(2800, 2.90)$ for $m = 4$ RW, and $(2150, 3.50)$ for $m = 3$ RW.

ranges, [8] have predicted primary bifurcations to rotating waves (RW) with azimuthal wavenumber $m = 2, 3$, or 4 . Figure 1 shows a three-dimensional perspective of isosurfaces of the perturbation in the axial velocity, w_p , (obtained by setting the $m = 0$ contribution to w to zero), for these three RW states at parameter values $(Re, \Lambda) = (2750, 1.58)$ for the $m = 2$ RW, $(2800, 3.00)$ for the $m = 4$ RW, and $(2150, 3.50)$ for the $m = 3$ RW. These figures show the interlaced spiral structures associated with the bifurcated modes. Contours of w_p for these three cases are also presented in Fig. 2, which clearly shows the symmetric structure of these pure rotating waves. In these states, the spatial structure is stationary in a frame rotating with the precession frequency. The parameter values where these various RW states bifurcate, their azimuthal wavenumbers, and their precession frequencies are in very good agreement with the prediction from linear stability analysis [8].

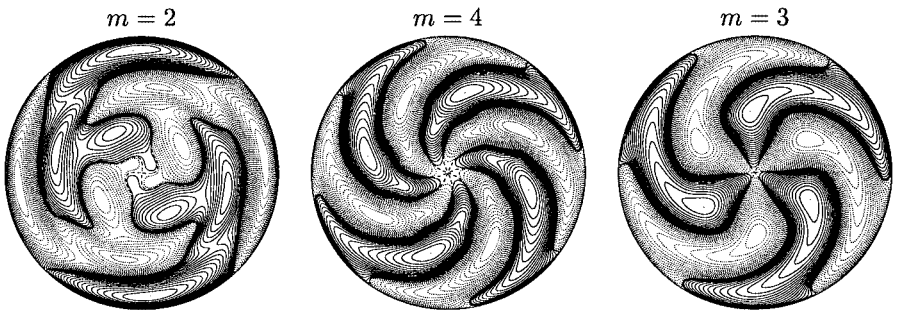


FIG. 2. Contours of w_p at $z = 0.8\Lambda$ for the pure rotating wave solutions shown in Fig. 1. Contour levels are $\max(w_p)(i/20)^2$, for $i \in [-20, 20]$, solid (dashed) lines are positive (negative).

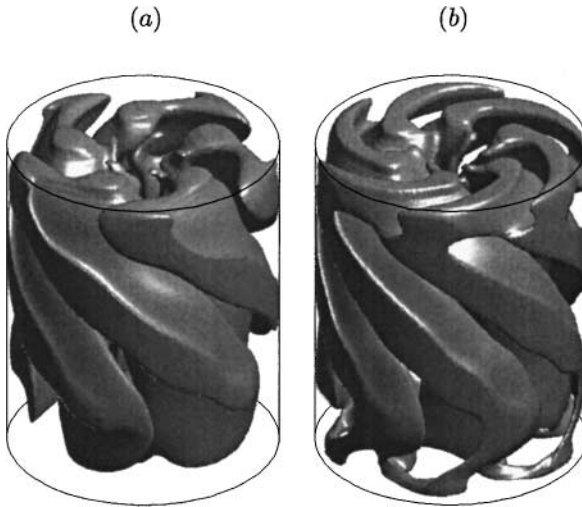


FIG. 3. Three-dimensional isosurfaces, near the zero level, of w_p for modulated rotating waves; (a) the ($m = 0, m = 5$) MRW at $Re = 3500$ and $\Lambda = 2.5$, and (b) the ($m = 0, m = 6$) MRW at $Re = 3700$ and $\Lambda = 2.5$.

In the range $1.6 < \Lambda < 2.8$, the primary bifurcation is to an axisymmetric time-periodic flow (a limit cycle), which has been described in detail in a variety of axisymmetric studies (e.g., [10, 11]). Secondary bifurcations give branches of solutions that break the $SO(2)$ symmetry, resulting in modulated rotating waves (MRW), which have a pure azimuthal wavenumber dependency together with a time-periodic $m = 0$ component, of period T , so that the pattern does not rotate rigidly, but changes with time. Since T and the precession period T_p of the $m = 6$ component are not commensurate, the pattern never repeats in a fixed reference frame, but is periodic in a frame, rotating with the precession period T_p (in this particular case, $T_p \approx 4.2T$). Figure 3 shows a three-dimensional perspective of isosurfaces of the perturbation to the axial velocity for MRW at ($Re = 3500, \Lambda = 2.5$) with $m = 5$ and at ($Re = 3700, \Lambda = 2.5$) with $m = 6$. Figure 4 comprises contours of the bifurcated pattern of w_p over one period ($T = 28.0$), for the ($m = 0, m = 6$) MRW at an axial level $z = 0.8\Lambda$.

Secondary bifurcations with a more complicated azimuthal structure have also been observed. For $\Lambda = 3.0$, the first bifurcation is to a RW with $m = 4$, and this RW undergoes a secondary bifurcation (Naimark–Sacker) where a second frequency associated with the $m = 1$ mode emerges. Figure 5 shows three-dimensional perspectives of the perturbation of the axial velocity for the ($m = 1, m = 4$) MRW. Parts (a) and (b) display isosurfaces of the $m = 1$ component; (a) has the isolevel at 10% of maximum, showing that all of the energy associated with this component is concentrated about the axis and is responsible for the precession of the vortex breakdown bubbles experimentally observed by Escudier [5]. Part (c) of the figure is the $m = 4$ component of this MRW and has the same structure as the pure $m = 4$ RW with $\Lambda = 3.0$ and lower $Re = 2850$, shown in Fig. 1; that RW is the solution from which the MRW bifurcated via a Naimark–Sacker bifurcation. Part (d) is a snapshot of the complete quasiperiodic MRW perturbation, showing the interplay of both $m = 1$ and $m = 4$ azimuthal components; with MRW the spatial structure never repeats.

Figure 6 shows contours of the perturbation of the vertical velocity, w_p , obtained by setting the $m = 0$ component of w to zero. It clearly indicates how the two azimuthal

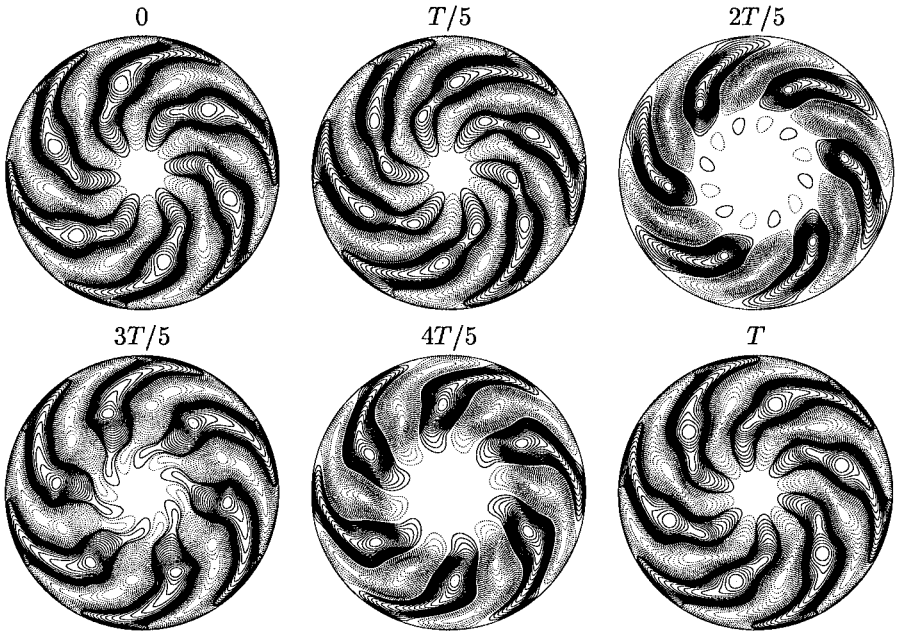


FIG. 4. Contours of w_p at $z = 0.8\Lambda$ for the modulated rotating wave solution shown in Fig. 3(b), over one period of the $m = 0$ component ($T = 28.0$). Contour levels are $\pm \max(w_p)(i/20)^2$, for $i \in [1, 20]$, solid (dashed) lines are positive (negative).

contributions $m = 1$ and $m = 4$ to the MRW are spatially separated. The $m = 4$ component is a jet mode associated with the maximum azimuthal velocity, and the $m = 1$ component is a core mode, located about the axis.

We use this MRW case, with the most complicated spatial structure incorporating the $m = 1$ mode that via the nonlinear terms couples to all azimuthal modes, to test the spectral convergence of the scheme. Figure 7 shows the kinetic energy associated with each azimuthal

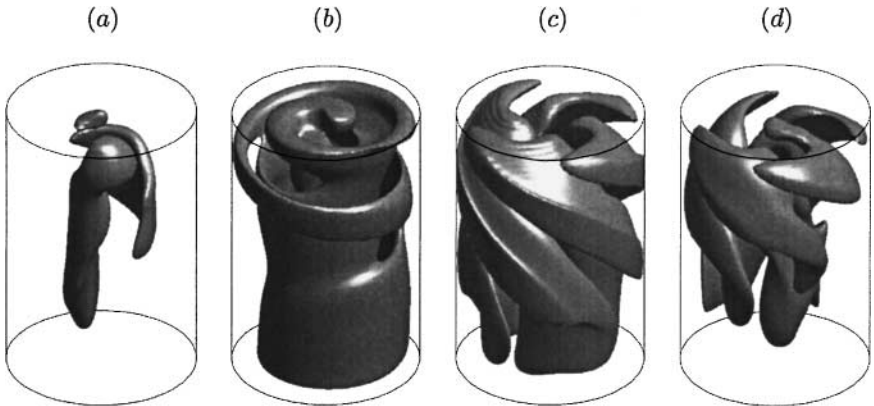


FIG. 5. Three-dimensional perspectives of the perturbations of the axial velocity for a modulated rotating wave solution corresponding to $Re = 2950$ and $\Lambda = 3.0$. Isosurfaces of the $m = 1$ mode, at (a) 10% of maximum and (b) close to zero, (c) isosurface of the $m = 4$ mode close to zero, and (d) isosurface of the axial velocity perturbation, w_p , at 20% of maximum showing the interplay of both $m = 1$ and 4 modes.

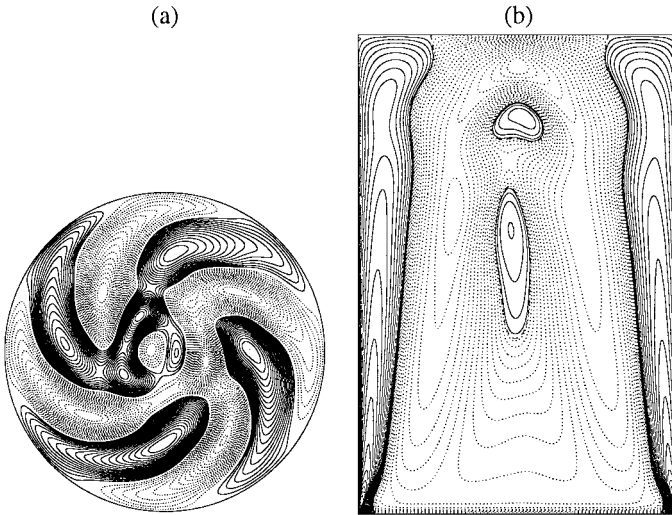


FIG. 6. Contours of (a) w_p at $z = 0.8\Lambda$ and (b) w at $\theta = 0$, for the $(m = 1, m = 4)$ MRW at $Re = 2950$ and $\Lambda = 3.0$. Contour levels are $\max(w)(i/20)^2$ for $i \in [-20, 20]$, solid (dashed) lines are positive (negative) levels.

mode, E_m , for solutions with 64 Legendre modes in r and z , and $L = 19, 27, 35$, and 43 (i.e., 10, 14, 18, and 22 azimuthal modes), where

$$E_m = \frac{1}{2} \int_0^H \int_0^R \int_0^{2\pi} \mathbf{u}_m \cdot \bar{\mathbf{u}}_m r \, d\theta \, dr \, dz.$$

The figure clearly demonstrates the spectral convergence of the scheme, and that for this problem, $L = 19$ captures the essence of the MRW, and increasing L beyond 27 results in virtually no change in the solution.

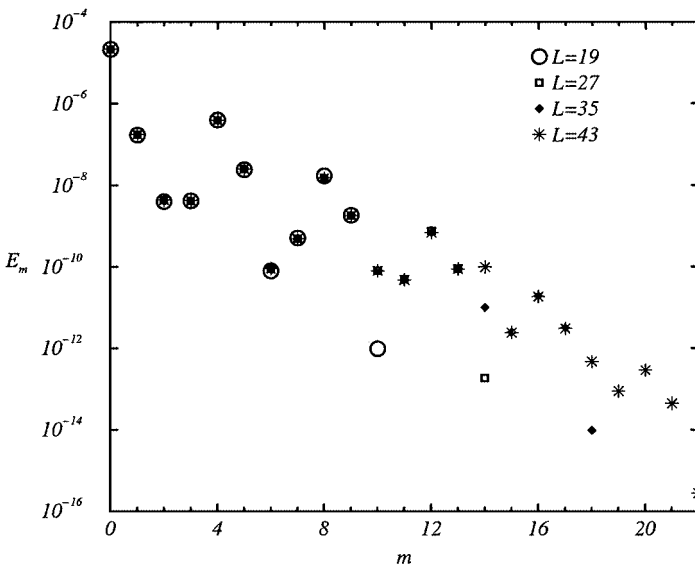


FIG. 7. Variations in E_m due to azimuthal resolution for the MRW case at $Re = 2900$, $\Lambda = 3.0$, using $N = M = 64$ modes in r and z , and L as indicated in θ .

In the test problem presented, a strong boundary layer develops at the rotating endwall, of thickness that scales with $Re^{-0.5}$. This boundary layer and the discontinuity of the boundary conditions at the corner where the rotating bottom meets the stationary sidewall place a significant demand on the spatial resolution in (r, z) . These characteristics of the test problem make finite difference/finite volume schemes impractical in three-dimensional computations and have been resolved here using 64 spectral modes in both r and z .

5. CONCLUDING REMARKS

We have presented a fast and accurate spectral-projection scheme for solving the three-dimensional Navier–Stokes equations in enclosed cylinders. We have successfully applied this code to the flow inside a cylinder with a rotating bottom endwall, and have obtained several bifurcated three-dimensional states, with complex spatial and temporal behavior, in good agreement with experiments.

In this problem there exist three points in parameter space where the basic state first loses stability as two pairs of complex conjugate eigenvalues simultaneously cross the imaginary axis; these double Hopf points act as organizing centers of the subsequent nonlinear dynamics [18]. The present code is playing a key role in unraveling the complicated dynamics associated with these codimension-2 bifurcations [16], and the transition to complex dynamics.

ACKNOWLEDGMENT

We thank Alvaro Meseguer for his help with the 3D plots. This work was supported by NSF Grants DMS-9706951, DMS0074283, INT-9732637, and CTS-9908599 (USA), DGICYT Grant PB97-0685, and DGU Grant 1999BEAI400103 (Spain).

REFERENCES

1. C. Bernardi, M. Dauge, and Y. Maday, *Spectral Methods for Axisymmetric Domains*, Éditions Scientifiques et Médicales Elsevier, Paris (Gauthier-Villars, 1999), numerical algorithms and tests due to Mejdî Azâez.
2. H. M. Blackburn and J. M. Lopez, Symmetry breaking of the flow in a cylinder driven by a rotating endwall, *Phys. Fluids* **12**, 2698 (2000).
3. J. P. Boyd, *Chebyshev and Fourier Spectral Methods* (Springer-Verlag, Berlin/New York, 1989).
4. C. Canuto, M. Y. Hussaini, A. Quarteroni, and T. A. Zang, *Spectral Methods in Fluid Dynamics* (Springer-Verlag, Berlin/New York, 1988).
5. M. P. Escudier, Observations of the flow produced in a cylindrical container by a rotating endwall, *Expt. Fluids* **2**, 189 (1984).
6. A. Y. Gelfgat, P. Z. Bar-Yoseph, and A. Solan, Stability of confined swirling flow with and without vortex breakdown, *J. Fluid Mech.* **311**, 1 (1996).
7. J. L. Guermond and J. Shen, 2001 On the error estimates of the pressure-correction scheme with a divergence correction, in preparation.
8. A. Y. Gelfgat, P. Z. Bar-Yoseph, and A. Solan, Three-dimensional instability of axisymmetric flow in a rotating lid-cylinder enclosure, *J. Fluid Mech.* **438**, 363 (2001).
9. W. Huang and D. M. Sloan, Pole condition for singular problems: The pseudospectral approximation, *J. Comput. Phys.* **107**, 254 (1993).
10. J. M. Lopez, Axisymmetric vortex breakdown. 1. Confined swirling flow, *J. Fluid Mech.* **221**, 533 (1990).

11. J. M. Lopez, F. Marques, and J. Sanchez, Oscillatory modes in an enclosed swirling flow, *J. Fluid Mech.* **439**, 109 (2001).
12. J. M. Lopez and A. D. Perry, Axisymmetric vortex breakdown. 3. Onset of periodic flow and chaotic advection, *J. Fluid Mech.* **234**, 449 (1992).
13. J. M. Lopez and J. Shen, An efficient spectral-projection method for the Navier–Stokes equations in cylindrical geometries I. Axisymmetric cases, *J. Comput. Phys.* **139**, 308 (1998).
14. F. Marques, On boundary conditions for velocity potentials in confined flows. Application to Couette flow, *Phys. Fluids A* **2**, 729 (1990).
15. F. Marques and J. M. Lopez, Precessing vortex breakdown mode in an enclosed cylinder flow, *Phys. Fluids* **13**, 1679 (2001).
16. F. Marques, J. M. Lopez, and J. Shen, Mode interactions in an enclosed swirling flow: A double Hopf bifurcation between azimuthal wavenumbers 0 and 2, *J. Fluid Mech.* **455**, 263 (2002).
17. T. Matsushima and P. S. Marcus, A spectral method for polar coordinates, *J. Comput. Phys.* **120**, 365 (1995).
18. T. Mullin, *The Nature of Chaos* (Oxford Univ. Press, London, 1993).
19. S. A. Orszag and A. T. Patera, Secondary instability of wall-bounded shear flows, *J. Fluid Mech.* **128**, 347 (1983).
20. J. C. F. Pereira and J. M. M. Sousa, Confined vortex breakdown generated by a rotating cone, *J. Fluid Mech.* **385**, 287 (1999).
21. V. G. Priymak and T. Miyazaki, Accurate Navier–Stokes investigation of transitional and turbulent flows in a circular pipe, *J. Comput. Phys.* **142**, 370 (1998).
22. S. Rüdiger and F. Feudel, Pattern formation in Rayleigh–Bénard convection in a cylindrical container, *Phys. Rev. E* **62**, 4927 (2000).
23. J. Shen, Efficient spectral–Galerkin method I. Direct solvers for second- and fourth-order equations by using Legendre polynomials, *SIAM J. Sci. Comput.* **15**, 1489 (1994).
24. J. Shen, Efficient Chebyshev–Legendre Galerkin methods for elliptic problems, in *Proceedings of ICOSA-HOM’95* edited by A. V. Ilin and R. Scott (*Houston J. Math.*, 1996).
25. J. Shen, Efficient spectral–Galerkin methods. III. Polar and cylindrical geometries, *SIAM J. Sci. Comput.* **18**, 1583 (1997).
26. F. Sotiropoulos and Y. Ventikos, The three-dimensional structure of confined swirling flows with vortex breakdown, *J. Fluid Mech.* **426**, 155 (2001).
27. J. L. Stevens, J. M. Lopez, and B. J. Cantwell, Oscillatory flow states in an enclosed cylinder with a rotating endwall, *J. Fluid Mech.* **389**, 101 (1999).
28. L. J. P. Timmermans, P. D. Mineev, and F. N. Van De Vosse, An approximate projection scheme for incompressible flow using spectral elements, *Int. J. Numer. Methods Fluids* **22**, 673 (1996).
29. L. S. Tuckerman, Divergence-free velocity fields in nonperiodic geometries, *J. Comput. Phys.* **80**, 403 (1989).
30. R. Verzicco and P. Orlandi, A finite-difference scheme for three-dimensional incompressible flows in cylindrical coordinates, *J. Comput. Phys.* **123**, 402 (1996).